Experimental Three-Dimensional Velocity Data of a Sweeping Jet from a Fluidic Oscillator Interacting with a Crossflow

F. Ostermann, R. Woszidlo, C.N. Nayeri, and C.O. Paschereit

Hermann-Föttinger-Institut
Technische Universität Berlin

September 28, 2018

Introduction

Jets in crossflow are a fundamental flow scenario for a variety of technical applications (e.g., chimneys, fuel injection, and flow control). Especially in flow control, spatially oscillating jets (i.e., sweeping jets) emitted from fluidic oscillators into a crossflow have proven to be effective in, for example, mixing enhancement [1], separation control [2], drag reduction [3], and film cooling [4]. Fluidic oscillators are devices that are able to generate spatially and/or temporally oscillating jets without the need of moving parts because the oscillation is solely caused by the internal flow dynamics. However, the driving mechanisms behind the effectiveness of fluidic oscillators in flow control have remained unclear because the fundamental flow field dynamic is unknown. The main reasons for this shortcoming are the requirements for a high spatial and concurrently high temporal resolution for understanding the complex interactions within the three-dimensional flow field.

As far as the authors are aware, the included dataset is the first experimentally acquired data that captures the quasi-time-resolved, three-dimensional flow field of a spatially oscillating jet interacting with an attached crossflow over a flat plate. It served as the basis for several publications [5–7], one video awarded with the Milton-van-Dyke award [8], and one PhD thesis [9]. Furthermore, the data has been consulted for validation of CFD studies [10,11].

The dataset is published in order to offer a basis for future studies on spatially oscillating jets in crossflow for other researchers and enable a simple access to the data for validation of CFD studies. Furthermore, it is a suitable dataset for testing new data analysis and visualization approaches.

Experimental Setup

Most experimental details are described in the associated publications. Here, only the main facts are summarized and additional details are provided that may be of particular interest when working with the provided data.

The experiments were conducted in an open return wind tunnel at the Hermann-Föttinger-Institut of the Technische Universität Berlin in the years 2016–2018. A schematic of the wind tunnel is illustrated in figure 1. The wind tunnel is able to provide velocities up to 25 m/s at a turbulence level of 0.15%. The wind tunnel velocity is measured using a Pitot-static tube. The measurement section is 2.5 m long and has a cross-section of $55 \times 55\,\mathrm{cm}^2$. An adjustable ceiling allows to modify the streamwise pressure gradient (figure 1, 7). For the presented dataset, this gradient is set to zero. A splitter plate is installed inside the measurement section to build up a fresh boundary layer (figure 1, 6). The splitter plate reduces the height of the measurement section to approximately 35 cm. The boundary layer is a fully turbulent flat plate boundary layer. At the position of the jet injection, its 99%-thickness is 16 mm on average and its momentum thickness is 1.6 mm. Depending on the crossflow velocity, the 99%-thickness varies between 13 and 19 mm. The boundary layer velocity profiles were measured using a Pitot tube with a diameter of 0.3 mm. The boundary layer profiles for three crossflow velocities are provided in the folder `boundaryLayer`. The individual UTF-8 encoded csv-files include the measurement settings, ambient conditions, and the streamwise velocities at various distances from the splitter plate.

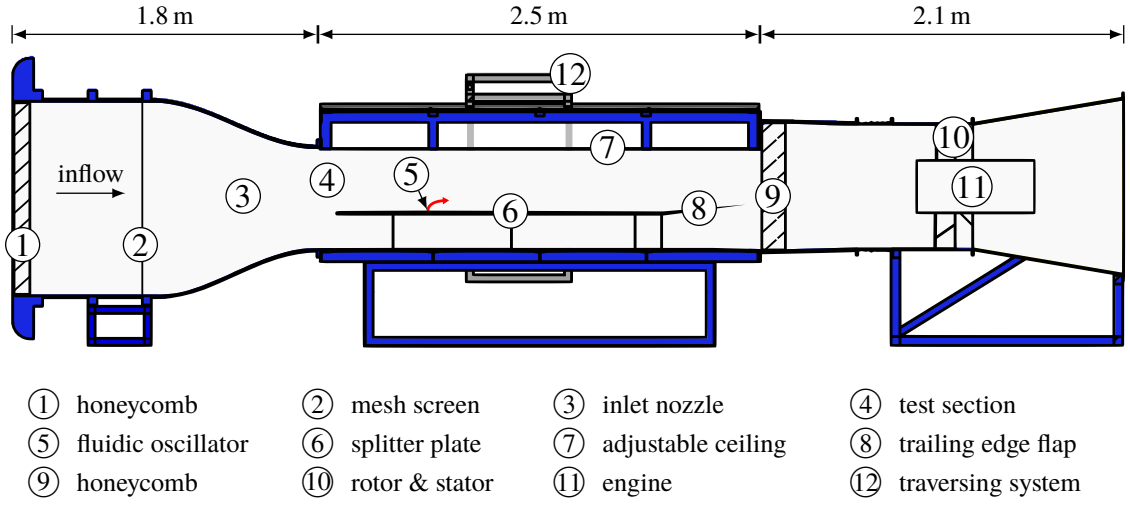

Figure 1: Schematic of the employed wind tunnel.[9]

The spatially oscillating jet is created by a fluidic oscillator with two feedback channels. The employed geometry of the oscillator is provided along with the presented dataset as a step file (`fluidic_oscillator.STEP`). The geometry is based on a patent by Stouffer and Bower[12]. The flow dynamics inside the oscillator are investigated by Ostermann et al.[13] and Sieber et al.[14]. The

outlet nozzle throat of the oscillator is $10 \times 10\,\mathrm{mm}^2$. The oscillator is installed inside the splitter plate. Its installation angles are chosen so that the virtual plane spanned by the sweeping jet is perpendicular to the direction of the crossflow (i.e., 90 deg injection angle and no skew angle). The supply rate of the oscillator is provided by a massflow controller. The velocity ratio R is defined as the ratio between the theoretical bulk jet velocity U_{bulk} and the crossflow velocity U_∞ (Eq. 1). The bulk velocity is determined from the supplied massflow $\dot{m}_{supply}$ assuming ambient conditions (i.e., the ambient density ρ_0) and a top-hat velocity profile at the nozzle throat with the outlet area $A_{outlet}(Eq.\ 2)$.

$$R = \frac{U_{bulk}}{U_\infty} \tag{1}$$

$$U_{bulk} = \frac{\dot{m}_{supply}}{\rho_0 A_{outlet}} \tag{2}$$

It is important to note that the inertia of the fluid supply chain does not allow for compensating temporal oscillations in the supply rate. Hence, the provided massflow is the time-averaged massflow. Earlier studies revealed that the massflow exiting the nozzle oscillates temporally due to an oscillating counter-pressure.[13] Although these oscillations are small (of the order of 10%), this may cause discrepancies between the dataset and numerical simulations that assume a constant supply rate as a boundary condition at the inlet.

The velocity data is acquired by employing a stereoscopic particle image velocimetry (PIV) system. The PIV system is able to capture the three-dimensional velocities inside a two-dimensional plane at a sampling rate of 6 Hz. A traversing system enables to move the complete PIV system in the streamwise and the spanwise direction. This allows for acquiring the three-dimensional velocity field plane-by-plane. The acquired data extends approximately 165 mm in the crossflow streamwise direction, 140 mm in the direction normal to the wall, and up to 120 mm in the spanwise direction. The extent of the volume is doubled when considering the symmetry of the flow field, which is explained later. The individually measured planes are oriented in the streamwise and the wall-normal direction. The spanwise direction is sampled by up to 22 planes. For each plane, up to 8000 flow field snapshots are recorded. Therefore, the acquisition of each three-dimensional flow field results in more than five terabytes of data. Added to that are around 25 days of computing time required for extracting the instantaneous velocity fields. Accordingly, the complete included dataset (i.e., four three-dimensional flow fields) is extracted from 20 terabytes of raw data, which took approximately 100 days of computing time. The snapshots were evaluated using PIVView3C by PIVTec.

The velocity fields are phase-averaged in order to eliminate stochastic noise, compensate for the small PIV sampling rate, and provide a temporal correlation between the individually measured planes. The data is phase-averaged based on a reference signal as suggested and validated by Ostermann et al.[15] for an oscillating flow field of a fluidic oscillator. The reference signal is extracted from simultaneously conducted pressure measurements inside the oscillator. The reference signal is used for identifying the individual oscillation periods. This information is used to assign one phase-angle

to each PIV snapshot. All snapshots within a phase-angle window are averaged. The oscillation period is divided into 120 phase-angle windows with a window size of 3 deg. The starting point of the oscillation period is chosen somehow arbitrarily but consistently between the individual measurements. It is set to zero pressure difference between the feedback channel inlets, which approximately coincides with the jet leaving the nozzle at zero deflection. This phase-averaged pressure difference is provided in the `pressureData.csv` of each measured scenario. The positions of the pressure sensors are marked by small cylinders located at the oscillator wall in `fluidic_oscillator.STEP`.

It is noteworthy that only half of the symmetric flow field is captured and included in the dataset (i.e., $z > 0$). The other half of the flow field is obtainable by accounting for the symmetry and the phase-lag between both sides $\Delta\phi = 180°$ (Eq. 3).

$$\begin{pmatrix} u(x, y, -z, \phi) \\ v(x, y, -z, \phi) \\ w(x, y, -z, \phi) \end{pmatrix} = \begin{pmatrix} u(x, y, z, \phi + 180°) \\ v(x, y, z, \phi + 180°) \\ -w(x, y, z, \phi + 180°) \end{pmatrix} \tag{3}$$

The measured data overlaps the plane of symmetry (i.e., the x-y-plane at $z = 0$) by up to 8 mm, which allows for a smooth transition between the measured and mirrored data. This smooth transition may be achieved by a weighted average of the symmetric and original data with a linear transition from only symmetric flow field at z_{min} of the overlap over the same weight at $z = 0$ to only original data at z_{max} of the overlap.

Data Format

The dataset includes the three-dimensional, quasi-time-resolved velocity fields of four scenarios. The key parameters of the scenarios are summarized in table 1. The flow fields of three different velocity ratios (i.e., R1, R3, and R5) and one different oscillation frequency at a given velocity ratio (i.e., T2) were measured.

name	velocity ratio	oscillation frequency	U_{bulk}	U_∞
R1	1.0	23.4 Hz	15.0 m/s	15.0 m/s
T2	3.0	34.1 Hz	22.5 m/s	7.50 m/s
R3	3.0	66.8 Hz	45.0 m/s	15.0 m/s
R5	5.0	72.1 Hz	50.0 m/s	10.0 m/s

Table 1: Included Scenarios

The ambient conditions during the measurements are provided in the respective file `conditions.txt` that is located in the folder of each scenario. The file `pressureData.csv` contains the pressure difference between two positions inside the oscillator that are marked as small cylinders in the file `fluidic_oscillator.STEP`. This pressure data is provided for the phase-alignment of other data to the presented dataset.

The text file `gridDefinition.txt` provides the dimensions and size of the structured grid of each scenario. The employed coordinate system origin is located in the middle of the oscillator outlet with $z = 0$ being located at the wall (i.e., the splitter plate). The coordinate x is oriented in the crossflow direction and the coordinate y is oriented normal to the wall. It is noteworthy that the grid is not the same between the scenarios. Furthermore, it is not uniformly spaced in the z-direction.

Each scenario contains a folder `data` that contains the data files. For each phase-angle, one corresponding data file is provided. In total, 120 phase-angles are provided for each scenario. The name of the files represent the phase-angles in degree. The files are comma-separated UTF-8 data files. Each line, beginning from the second line, contains one velocity vector with its components u, v, and w in m/s at a point x, y, and z in mm. The points are sorted by their coordinate. All points together form the aforementioned structured grid.

It is important to note that the provided precision of the numbers does neither represent the actual precision of the measured velocities nor account for the uncertainty of the PIV measurements. Although the data is provided at a precision of 1/100th of 1 m/s, the PIV measurement uncertainty is expected to be considerably higher. However, the uncertainty has not been quantified because, so far, no reliable nor convenient procedure of quantifying the uncertainty of stereoscopic PIV measurements exist.

Investigating the three-dimensional, quasi-time-resolved flow field requires post-processing tools that are able to handle the amount of data. One quick possibility for a first exploration using ParaView 5.5.0[16] is described in the following:

1. Extract the dataset by using any appropriate extraction tool (e.g., 7zip, gzip).
2. Open one of the csv-files with paraview. It should now parse the file inside a table.
3. Select the table in the *Pipeline Browser* and click *Filters* → *Alphabetical* → *Table To Structured Grid*. Ignore the error messages that may pop up.
4. Inside the *Properties*-window choose `x(mm)` as *X Column*, `y(mm)` as *Y Column*, and `z(mm)` as *Z Column*. Furthermore, enter the grid-size provided in the corresponding `gridDefinition.txt` to the *Whole Extent*-text fields. For example, for `x_size=186`, `y_size=126`, and `z_size=25`, as noted in the `gridDefinition.txt` enter:

Whole Extent	`0`	`185`
	`0`	`125`
	`0`	`24`

5. Click on *Apply* if necessary and change the visibility of the new added object to visible in the *Pipeline-Browser*. Now it is save to clear all errors because no new one should pop up.

6. In order to merge the three scalars u, v, and w to a vector, add a calculator filter (*Filters* → *Common* → *Calculator*). In the formula text field enter:

```
u(m/s)*iHat + v(m/s)*jHat + w(m/s)*kHat
```

7. One phase-angle of the data is now successfully added. Consult the ParaView documentation or the multitude of available tutorials for further steps to explore the data.

Recall that only one half of the flow field is included in the provided data. The other half needs to be reproduced with Eq. 3 using any post-processing tool. Generally, it is recommended to read the data with a post-processing tool of your choice and save the data again in an appropriate binary format because this most likely reduces the loading times significantly.

Another possibility for a more quantitative investigation of the flow field is for example provided by Matlab[17]. The following code snippets imports data from one timestep using Matlab 2017b:

```
% import csv file
data = csvread(fullfile(path_to_files,'000.csv'),1,0);

% reshape to grid using the information from the gridDefinition.txt
% for example x_size=186, y_size=126, and z_size=25
x = reshape(data(:,1),[186,126,25]);
y = reshape(data(:,2),[186,126,25]);
z = reshape(data(:,3),[186,126,25]);
u = reshape(data(:,4),[186,126,25]);
v = reshape(data(:,5),[186,126,25]);
w = reshape(data(:,6),[186,126,25]);
```

Of course, the same procedure is also transferable to other programming languages. Note that this code reads the data in `ndgrid`-format. For `meshgrid`-format an additional rearrangement of dimensions is necessary. This code snippet only imports one half of the flow field that is captured in the data. The other half may be obtained following Eq. 3.

Associated Publications

The provided data is part of the discussions in following publications:

F. Ostermann, R. Woszidlo, C. N. Nayeri, and C. O. Paschereit. The time-resolved flow field of a jet emitted by a fluidic oscillator into a crossflow. In *54th AIAA Aerospace Sciences Meeting*. American Institute of Aeronautics and Astronautics, Jan 2016. doi:10.2514/6.2016-0345.

F. Ostermann, R. Woszidlo, C. N. Nayeri, and C. O. Paschereit. Effect of velocity ratio on the flow field of a spatially oscillating jet in crossflow. In *55th AIAA Aerospace Sciences Meeting*. American Institute of Aeronautics and Astronautics, Jan 2017. doi:10.2514/6.2017-0769.

F. Ostermann, P. Godbersen, R. Woszidlo, C. N. Nayeri, and C. O. Paschereit. Sweeping jet from a fluidic oscillator in crossflow. *Physical Review Fluids*, 2(9), Sep 2017. doi:10.1103/physrevfluids.2.090512.

F. Ostermann, R. Woszidlo, C. N. Nayeri, and C. O. Paschereit. The interaction between a spatially oscillating jet emitted by a fluidic oscillator and a crossflow. *Journal of Fluid Mechanics (under revision)*, 2018.

F. Ostermann. Fundamental properties of a spatially oscillating jet emitted by a fluidic oscillator. *Doctoral Thesis at the Technische Universität Berlin*, 2018. doi:10.14279/depositonce-7144.

Acknowledgements

This work was funded by the Deutsche Forschungsgemeinschaft (DFG Project 289230680), which the authors gratefully acknowledge. Furthermore, the authors are thankful for the team of the Hermann-Föttinger-Institut and the students (particularly Marc Feldwisch, Sascha Martinke, Philipp Godbersen, and Edgar Roch) that contributed a significant amount of work to the setup of the experiments and data acquisition.

References

[1] A. Lacarelle and C. O. Paschereit. Increasing the passive scalar mixing quality of jets in crossflow with fluidics actuators. *Journal of Engineering for Gas Turbines and Power*, 134(2): 021503, 2012. doi:10.1115/1.4004373.

[2] R. Seele, P. Tewes, R. Woszidlo, M. A. McVeigh, N. J. Lucas, and I. J. Wygnanski. Discrete Sweeping Jets as Tools for Improving the Performance of the V-22. *AIAA Journal of Aircraft*, 46(6):2098–2106, 2009. doi:10.2514/1.43663.

[3] H.-J. Schmidt, R. Woszidlo, C. N. Nayeri, and C. O. Paschereit. Drag reduction on a rectangular bluff body with base flaps and fluidic oscillators. *Experiments in Fluids*, 56(7), Jul 2015. ISSN 1432-1114. doi:10.1007/s00348-015-2018-3.

[4] M. A. Hossain, R. Prenter, R. K. Lundgreen, A. Ameri, J. W. Gregory, and J. P. Bons. Experimental and numerical investigation of sweeping jet film cooling. *Journal of Turbomachinery*, 140(3):031009, Dec 2017. doi:10.1115/1.4038690.

[5] F. Ostermann, R. Woszidlo, C. N. Nayeri, and C. O. Paschereit. The time-resolved flow field of a jet emitted by a fluidic oscillator into a crossflow. In *54th AIAA Aerospace Sciences Meeting*. American Institute of Aeronautics and Astronautics, Jan 2016. doi:10.2514/6.2016-0345.

[6] F. Ostermann, R. Woszidlo, C. N. Nayeri, and C. O. Paschereit. Effect of velocity ratio on the flow field of a spatially oscillating jet in crossflow. In *55th AIAA Aerospace Sciences Meeting*. American Institute of Aeronautics and Astronautics, Jan 2017. doi:10.2514/6.2017-0769.

[7] F. Ostermann, R. Woszidlo, C. N. Nayeri, and C. O. Paschereit. The interaction between a spatially oscillating jet emitted by a fluidic oscillator and a crossflow. *Journal of Fluid Mechanics (under revision)*, 2018.

[8] F. Ostermann, P. Godbersen, R. Woszidlo, C. N. Nayeri, and C. O. Paschereit. Sweeping jet from a fluidic oscillator in crossflow. *Physical Review Fluids*, 2(9), Sep 2017. doi:10.1103/physrevfluids.2.090512.

[9] F. Ostermann. Fundamental properties of a spatially oscillating jet emitted by a fluidic oscillator. *Doctoral Thesis at the Technische Universität Berlin*, 2018. doi:10.14279/depositonce-7144.

[10] M. A. Hossain, R. Prenter, R. K. Lundgreen, L. Agricola, A. Ameri, J. W. Gregory, and J. P. Bons. Investigation of crossflow interaction of an oscillating jet. In *55th AIAA Aerospace Sciences Meeting*. American Institute of Aeronautics and Astronautics, Jan 2017. doi:10.2514/6.2017-1690.

[11] S. Aram, H. Shan, F. Ostermann, and R. Woszidlo. Computational validation and analysis of interaction of a sweeping jet and an attached turbulent flow. In *2018 AIAA Aerospace Sciences Meeting*. American Institute of Aeronautics and Astronautics, Jan 2018. doi:10.2514/6.2018-1798.

[12] Ronald D. Stouffer and Robert Bower. Fluidic flow meter with fiber optic sensor. Patent US 5827976, 1998.

[13] F. Ostermann, R. Woszidlo, C. Nayeri, and C. O. Paschereit. Experimental Comparison between the Flow Field of Two Common Fluidic Oscillator Designs. *53rd AIAA Aerospace Sciences Meeting*, January 2015. doi:10.2514/6.2015-0781.

[14] M. Sieber, F. Ostermann, R. Woszidlo, K. Oberleithner, and C. O. Paschereit. Lagrangian coherent structures in the flow field of a fluidic oscillator. *Physical Review Fluids*, 1(5), 2016. ISSN 2469-990X. doi:10.1103/PhysRevFluids.1.050509.

[15] F. Ostermann, R. Woszidlo, C. N. Nayeri, and C. O. Paschereit. Phase-Averaging Methods for the Natural Flowfield of a Fluidic Oscillator. *AIAA Journal*, 53(8):2359–2368, Aug 2015. ISSN 1533-385X. doi:10.2514/1.j053717.

[16] Kitware, Inc. Paraview. URL `https://www.paraview.org`.

[17] MathWorks. Matlab. URL `http://www.mathworks.com/products/matlab.html`.